

Accurate Extraction of Brillouin Frequency Shift using Single Deep Neural Network in BOTDA Sensing System with Non-Local Effect

Yuhao Qian, Guijiang Yang, Keyan Zeng, Liang Wang,* Ming Tang, and Deming Liu

National Engineering Laboratory for Next Generation Internet Access System, School of Optics and Electronic Information & Wuhan National Lab for Optoelectronics (WNLO), Huazhong University of Science and Technology, Wuhan 430074, China

*E-mail: hustwl@hust.edu.cn

Abstract: A single DNN model has been developed for accurate extraction of both Brillouin frequency shift without and with NLE. The scheme is practical and greatly improves the system tolerance to NLE without any hardware modification. © 2022 The Author(s)

1. Introduction

As one powerful method for distributed temperature and strain sensing, the Brillouin Optical Time Domain Analysis (BOTDA) sensing system has advantages of long sensing distance, high spatial resolution and good accuracy [1, 2]. However, some detrimental effects limit further increase of its sensing distance [3]. The non-local effect (NLE) is one of those detrimental effects originating from the pump depletion due to accumulated power transfer between the pump pulse and the continuous-wave (CW) probe along the fiber [4]. It distorts the Brillouin gain spectrum (BGS) and causes fatal measurement errors [5]. Several techniques have been proposed to overcome the NLE, such as dual-sideband scheme [6], laser wavelength modulation [7], combination with backward Rayleigh light [8], novel frequency scanning [9] and optical chirp chain probe [10]. However, those methods make the system complicated and expensive. In 2020, C. Lu et al. used artificial neural network (ANN) to retrieve the Brillouin frequency shift (BFS) with NLE [11]. Nevertheless, it requires two different ANN models to process the data without NLE and with NLE, which is not practical since it needs prior knowledge on whether the data has NLE or not.

In this work, a single deep neural network (DNN) model has been proposed to accurately extract the BFS for both the data without NLE and with NLE, without the need of prior knowledge of the data. Using the depletion factor of the pump pulse, a BGS expression under different NLE has been derived for the training of the DNN, which establishes the relationship between the input BGS and the output BFS, and realizes accurate extraction of the BFS no matter whether NLE exists or not in the system.

2. Principle and simulation

Here we consider the Brillouin gain configuration where the pump pulse is depleted when propagating along the fiber. ν is the frequency difference between the pump and probe, and a small fiber section at the end of the fiber under test (FUT) is heated, leading to a BFS change of $\delta\nu$ with respect to the unheated fiber section. The depletion factor d and the depleted pump intensity at the FUT end can be expressed as [12]:

$$d = (P_{P0} - P) / P_{P0} \quad (1) \quad I_p(\nu) = I_{P0} \exp \left[-\frac{d}{1 + 4(\nu - \nu_B)^2 / \Delta\nu_B^2} \right] \quad (2)$$

where P_{P0} is the pump power in absence of the probe light, P is the minimum power of the depleted pump, $\Delta\nu_B$ is the linewidth of the BGS and I_{P0} is the intensity of the pump pulse without Brillouin interaction. The Lorentzian BGS $g(\nu)$ is given in Eq. (3). Using Eqs. (1-3), the BGS at the heated section can be derived as Eq. (4):

$$g(\nu) = g_B \frac{\Delta\nu_B^2}{4(\nu - \nu_B)^2 + \Delta\nu_B^2} \quad (3) \quad g_{NLE}(\nu) = g(\nu - \delta\nu) \exp \left[-\frac{d}{1 + 4(\nu - \nu_B)^2 / \Delta\nu_B^2} \right] \quad (4)$$

where g_B is the Brillouin gain coefficient. When $\delta\nu$ is zero or large enough, the system will not suffer from NLE.

Using the above equations, we carry out the simulation for 25km long FUT. Fig. 1(a) shows the relationship between the depletion factor and input probe power. Larger probe power results in higher d and hence larger NLE. Fig. 1(b) gives the depleted pump power at the far end of the FUT ($\nu_B=10.850$ GHz, $\Delta\nu_B=30$ MHz). Fig. 1(c) and (d) show the distorted BGS induced by NLE under different d and $\delta\nu$, respectively. Compared with the normal BGS without NLE, the BGS with NLE (NLE-BGS) has a double-peak profile when the depletion factor is large. It is worth mentioning that when $\delta\nu$ is equal to one third of the BGS linewidth ($\delta\nu=10$ MHz in our case), the strength of NLE become maximum [12]. For those distorted BGS, using conventional Lorentzian curve fitting (LCF) method cannot accurately extract the BFS and would lead to large measurement errors.

Here we propose to use single DNN model to accurately extract BFS from both the normal BGS and

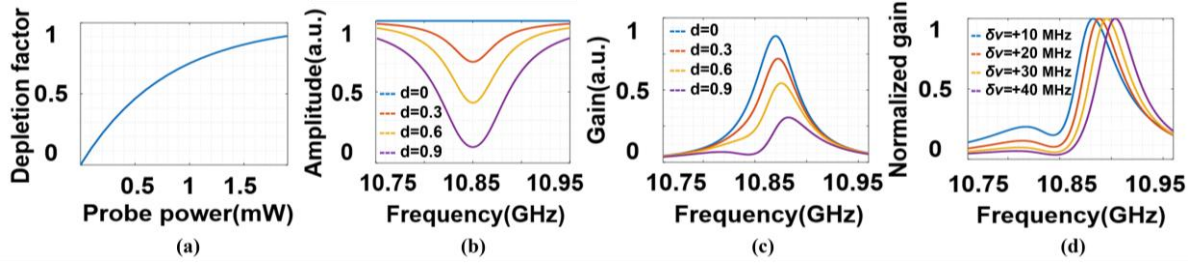


Fig. 1 (a) Depletion factor d vs input probe power; (b) depleted pump power vs ν ; (c) distorted BGS by NLE for different d when $\delta\nu=10$ MHz; (d) distorted BGS by NLE for different $\delta\nu$ when $d=0.9$.

distorted NLE-BGS. The input layer and output layer of the DNN have 200 and 1 neurons, corresponding to the number of data points on the BGS and the one output of BFS. To achieve correct BFS extraction for both conditions without and with NLE, the training dataset for DNN needs to cover different depletion factors. A wide range of the BGS linewidth, BFS variation and the SNR should also be taken into consideration. We generate the training dataset based on Eq. (4), where the d varies from 0 to 1 with a step of 0.1, $\Delta\nu_B$ varies from 25 MHz to 80 MHz with a step of 1 MHz and $\delta\nu$ varies from -2 MHz to 102 MHz with a step of 1 MHz. Moreover, the dataset is doubled by adding Gaussian noise to the clean ones to produce the data with 15dB SNR in order to improve the robustness of the DNN. 15dB SNR is selected for training since we find that the DNN model has good robustness during our test compared with other values of SNR. Finally, a dataset containing 129360 BGSs is formed, in which the ratio for dataset of training, test and validation is 7:2:1. After lots of trial and test, the number of neurons in the two hidden layers is set to be 60 and 15, respectively.

Fig. 2 shows the BFS change distribution extracted from simulated data ($\nu_B=10.850$ GHz, $\Delta\nu_B=30$ MHz) by using LCF and DNN, respectively. d is set to be 0.9 and $\delta\nu$ varies from 0MHz to 30MHz. In Fig. 2 (a), the BFS changes extracted by both methods are almost the same and are equal to the real BFS when the BFS is uniform along the whole FUT. This is because the pump depletion does not induce any error if the BFS is uniform [12]. Once there is a BFS change at the end of the FUT, as shown in Fig. 2 (b)-(d), the values of the BFS change extracted by LCF deviate from the real ones while those by DNN are still accurate. It is also seen that when $\delta\nu=10$ MHz the deviation is maximum, as shown in Fig. 2(b). It is worth mentioning that for unheated section our DNN model still works well and provides accurate BFS values as those by LCF, as shown in Fig. 2. Table 1 summarizes the root mean square error (RMSE) of the BFS extracted by LCF and DNN under different d and $\delta\nu$, respectively. For both DNN and LCF, when the depletion factor is larger, the RMSE increases due to larger NLE. Similarly, when $\delta\nu=10$ MHz, most of the RMSE values reach maximum as the NLE becomes larger when the BFS change is equal to one third of the BGS linewidth. However, for all the cases, the RMSE by DNN is always below 1 MHz, and in the worst scenario of NLE ($d=0.9$, $\delta\nu=10$ MHz) the RMSE by DNN is 14.8 times lower than that by LCF, showing that the proposed DNN model is capable of more accurate BFS extraction for both cases without NLE and with NLE.

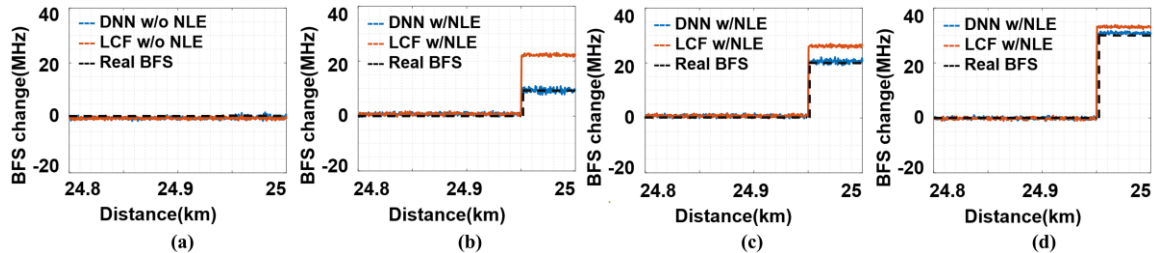


Fig. 2 Simulated BFS change distribution around the end of FUT extracted by LCF and DNN when $d=0.9$: (a) $\delta\nu=0$ MHz; (b) $\delta\nu=10$ MHz; (c) $\delta\nu=20$ MHz; (d) $\delta\nu=30$ MHz.

Table 1. Comparison of the Root mean square error (RMSE) of the BFS extracted by LCF and DNN

d	$\delta\nu=10$ MHz		$\delta\nu=20$ MHz		$\delta\nu=30$ MHz	
	LCF	DNN	LCF	DNN	LCF	DNN
0	0.2 MHz	0.42 MHz	0.3 MHz	0.45 MHz	0.2 MHz	0.43 MHz
0.3	2.1 MHz	0.20 MHz	1.4 MHz	0.28 MHz	0.9 MHz	0.25 MHz
0.6	4.8 MHz	0.63 MHz	2.3 MHz	0.38 MHz	1.5 MHz	0.30 MHz
0.9	12.0 MHz	0.81 MHz	4.9 MHz	0.67 MHz	2.5 MHz	0.52 MHz

3. Experiment and results

We use a single-sideband BOTDA setup [11] to verify our idea since the NLE can be easily observed in single-

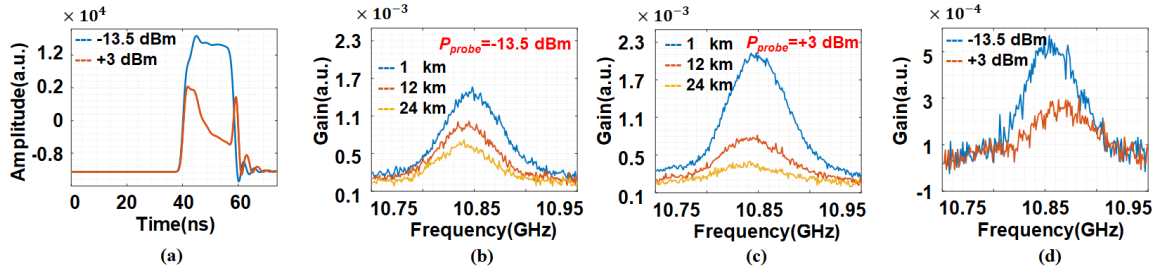


Fig. 3 (a) Pump pulses after transmission through the FUT; (b) BGSs at different locations of the unheated section without NLE ($P_{probe}=-13.5$ dBm, $d=0$); (c) BGSs at different locations of the unheated section with NLE ($P_{probe}=+3$ dBm, $d=0.78$); (d) BGSs at the heated section for $P_{probe}=-13.5$ dBm and $P_{probe}=+3$ dBm, respectively.

sideband BOTDA. The proposed scheme can still work for double-sideband BOTDA. The FUT is a 25 km-long single mode fiber (SMF) with $\nu_B=10.850$ GHz and the last 50 m section is heated to 40 °C (room temperature 23 °C). A 20ns pump pulse whose peak power is boosted to 20 dBm is used. The probe light is detected and averaged by 1024-times. Fig. 3(a) shows the measured pump pulses under two input probe powers, respectively. When $P_{probe}=-13.5$ dBm, the profile of the received pump pulse is almost not changed except some power drop due to the fiber loss. And the depletion factor is zero which means there is no NLE in the system. While for $P_{probe}=+3$ dBm, the pump pulse is largely depleted and the depletion factor is calculated to be 0.78. Fig. 3(b) and (c) are the measured BGSs at three different locations of the unheated section when $P_{probe}=-13.5$ dBm and $P_{probe}=+3$ dBm, respectively. Fig. 3(d) compares the BGSs at the heated section for $P_{probe}=-13.5$ dBm and $P_{probe}=+3$ dBm, respectively, indicating that the NLE exists at large probe power and distort the BGS severely.

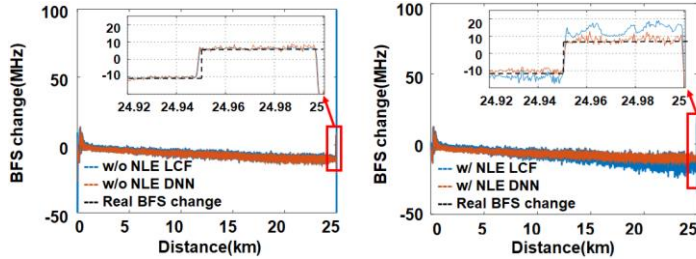


Fig. 4 BFS change distribution (a) without NLE (b) with NLE extracted by LCF (blue) and DNN (orange), respectively. Inset: zoom-in view.

Figure 4 shows the BFS change distribution without NLE ($P_{probe}=-13.5$ dBm) and with NLE ($P_{probe}=+3$ dBm) extracted by LCF and DNN, respectively. For the unheated section, the BFS distribution shows a decrease trend, which is caused by the uneven strain distribution on the fiber span. We can see that the BFS extracted by our DNN model always matches well with the real BFS change, no matter whether there is NLE or not. While the BFS extracted by LCF deviates from the real one, especially at the heated section with NLE existing, as shown in Fig. 4(b). The experimental RMSE of the BFS extracted by LCF and DNN is compared in Table 2. When $P_{probe}=-13.5$ dBm, the RMSEs by LCF and DNN are similar for both unheated and heated sections since there is no NLE in the system. While when $P_{probe}=+3$ dBm ($d=0.78$), the RMSE by DNN is over three times lower than that by LCF for both the unheated and heated sections. Especially at the heated section, the RMSE by LCF decreases to 8.84MHz, which indicates large measurement error induced by NLE. By using our DNN model, the RMSE is improved to be 2.57MHz, which shows that our DNN has large tolerance to NLE and can greatly enhance the measurement accuracy.

Table 2. Comparison of the experimental RMSE (MHz) of the BFS extracted by LCF and DNN

P_{probe} (dBm)	@unheated section		@heated section	
	LCF	DNN	LCF	DNN
-13.5	0.47	0.61	0.43	0.69
+3	3.14	1.01	8.84	2.57

4. Conclusion

We have proposed and demonstrated the use of single DNN model to accurately extract the BFS from both the normal BGS and distorted BGS by NLE. By using the depletion factor to reflect the strength of NLE together with a wide range of parameters of the NLE-BGS equation during the training process, the DNN improves the experimental measurement accuracy by three times compared with that of LCF. The proposed scheme is simple and practical to make BOTDA sensors have large tolerance to NLE without any modification of the hardware.

Acknowledgment

National Natural Science Foundation of China (62005087).

References

- [1] A. Motil, *et al.*, Optics & Laser Technol., 78, 81–103, (2016).
- [2] M. N. Alahbabli, *et al.*, Opt. Lett., 30(11), 1276–1278, (2005).
- [3] A. Loayssa, *et al.*, in Optical, Opto-Atomic, and Entanglement-Enhanced Precision Metrology, 19, (2019).
- [4] X.-H. Jia, *et al.*, J. Opt., 14(4), 045202, (2012).
- [5] C. Liu, *et al.*, OFC W2A.17 (2020).
- [6] R. Ruiz-Lombera, *et al.*, IEEE Photonics J., 7(6), 1–9, (2015).
- [7] J. Urricelqui, *et al.*, Opt. Exp., 22(15), 18195, (2014)
- [8] H. He, *et al.*, OFC M2J.7 (2019).
- [9] A. Dominguez-Lopez, *et al.*, Opt. Exp., 24(10), 10188 (2016).
- [10] Y. Dong, *et al.*, Opt. Lett., 43, 4679 (2018).
- [11] C. Lu, *et al.*, IEEE Sensors J., 20(15), 8559–8569, (2020).
- [12] L. Thévenaz, *et al.*, Opt. Exp., 21(12), 14017, (2013).